MPM Investigation of the Fluidization Initiation and Post-Fluidization Mechanism Around a Pressurized Leaking Pipe

Monzer, Ali; Faramarzi, Asaad; Yerro, Alba; Chapman, David

DOI:
10.1061/JGGEFK.GTENG-10985

MPM Investigation of the Fluidization Initiation and Post-Fluidization Mechanism Around a Pressurized Leaking Pipe

Ali Monzer[1], Asaad Faramarzi[2], Alba Yerro[3], and David Chapman[4]

[1]Ph.D. Candidate, Dept. of Civil Engineering, Univ. of Birmingham, Edgbaston, Birmingham, UK. Email: axm1369@student.bham.ac.uk

[2]Associate Professor, Dept. of Civil Engineering, Univ. of Birmingham, Edgbaston, Birmingham, UK. Email: a.faramarzi@bham.ac.uk

[3]Assistant Professor, Dept. of Civil and Environmental Engineering, Virginia Polytechnic Univ., Blacksburg, VA. Email: ayerro@vt.edu

[4]Professor, Dept. of Civil Engineering, Univ. of Birmingham, Edgbaston, Birmingham, UK. Email: d.n.chapman@bham.ac.uk

Abstract

Pipe leakage can induce soil fluidization resulting in severe consequences to the urban environment where underground buried pipes are extensively used. Soil fluidization is the process of transition of soil particles from solid-like to liquid-like behavior that can lead to the failure of the supporting ground and buried utilities. This paper applies the advanced two-phase double-point Material Point Method (MPM) technique to investigate the soil fluidization mechanism around a leaking pressurized water pipe embedded in fully saturated soil. In the model, the inflow water velocity leading to the initiation and evolution of soil fluidization around the leaking pipe is identified based on the changes in soil porosity and soil bed expansion ratio. This study shows that the MPM results are consistent with published experimental studies. Parametric analyses are presented to investigate the influence of different parameters, including the orifice size, bed height, and soil porosity on soil fluidization. The results show that the inflow velocity required for the onset and development of fluidization decreases with the increase in orifice size and soil porosity. The bed height increases the resistance of the soil bed against fluidization. The double-point MPM formulation is shown to be an effective and promising way to study soil-water interaction resulting from a leaking pipe. The model developed in this study can be used as a prediction tool to estimate the significance and progress of fluidization zone and to determine critical state that leads to ground failure. Such tool would be of significant value to asset managers that are responsible for maintenance of buried pipes, their supporting ground and surface transportation infrastructure.

Introduction

Non-revenue water (NRW) refers to the water produced that is not delivered to the intended consumers. These water losses can be physical losses induced by pipe leakage or apparent losses resulting from inaccuracies in metering, theft, or unmetered usage. Whilst water utilities in developed countries have sophisticated systems for monitoring apparent losses, most NRW loss occurs due to physical leaks and breaks. Water loss due to pipe leakage is a critical problem in many urban areas. According to a survey conducted by the Organization for Economic Co-operation and Development (OECD 2016), leakage rates range from 4% in Amsterdam to 65% in Mexico City. Poor construction, corrosion, external loading, poor maintenance, geological hazards, and seasonal changes can cause pipes to leak. According to the World Bank, the world pipe leakage amounts to over 8 billion US dollars in the annual revenue loss (Kingdom et al. 2006). In addition to losing water and revenue, leaks may cause damage to underground and surface infrastructure by weakening the surrounding soils (Waltham 1993). Often, this can cause significant financial damages or even fatal injuries (Rogers 2014).

Previous studies have shown that pipe leakage may result in soil fluidization if a sufficient leakage rate is present (Alsaydalani 2010; Li 2013). Soil fluidization is defined as the process by which soil particles lose their interlocking forces and turn into a viscous fluid or fluid-like state (Richards et al. 1990). This process initiates in the leak region as the effective stresses reduce to zero due to an increase in pore water pressure. Soil fluidization due to water leaking from underground water pipes can mobilize and displace the surrounding soil particles, generating an underground cavity in the region of the leakage (Guo et al. 2013). The formed cavity can continuously develop induced by leaking fluid, and the bed can be ruptured to the soil surface leading to a severe ground collapse (Tang et al. 2017). Considering the severity of the pipe leakage problem, it is essential to understand the water-soil interaction around a leak to maintain the safety of urban infrastructure.

Previous experimental studies have been conducted to predict the water loss induced by leakage (Germanopoulos et al. 1989; Lambert et al. 2001). These researches helped to develop different pressure-leakage models by proposing orifice flow equation. However, changes in the flow regime, pipe material behavior, and hydraulic fracturing increase the complexity of the interaction between the leaking pipe and the surrounding soil (van Zyl and Clayton 2007). A limited number of studies have focused on the pipe-leakage problem (Lennon et al. 1995; Awad and Karni 2000; Toshifumi et al. 2012). Experimental tests conducted by

Alsaydalani (2010) compared the ratio of total head loss through the orifice to that in the soil bed. The total head loss due to flow through the orifice was obtained by estimating the difference between the head upstream of the orifice and the head in the orifice. Alsaydalani observed that most of the energy losses occurred through the orifice (98% of the total energy losses) while a relatively small amount (2%) dissipated through the soil bed. This is consistent with Walski et al.'s (2006) experimental verification that total head losses due to Darcy's flow through the soil mass in the leakage problem are generally much smaller than that in the orifice in the leakage problem. van Zyl et al. (2013) conducted a series of experimental studies on fluidization induced by a vertical jet where they identified three zones in the vicinity of the leak: (a) a fluidized zone with mobilized soil particles caused by the water that extends from the region of the leak to the soil surface, (b) a mobile soil zone in which the particles are tightly packed, and (c) a static zone that might move but very slowly. Consistently, this study observed that most energy losses in the jet occurred through the orifice. van Zyl et al. (2013) also concluded that in some cases substantial pressure can be maintained within the leaking pipe without the fluidized zone reaching the soil surface.

Alsaydalani and Clayton (2013) adopted an experimental approach using a small-scale model to investigate the soil fluidization mechanism around a vertical jet emanating from a leak. In their tests, the leakage rate at the orifice into a granular soil layer was incrementally increased until the initiation of internal fluidization. It was observed that by increasing the flow rate, the excess pressure in the soil bed increased up to a peak point. Immediately after the peak, an abrupt drop in excess pore water pressure was associated with the onset of fluidization in the vicinity of the orifice. Alsaydalani and Clayton (2013) demonstrated that the onset of soil fluidization is controlled by the size of the particles, the particle shape, and the bed height. Using a set of experiment, He et al. (2017) showed the different soil fluidization stages associated with the increase in leakage rate through an upward water jet into a granular soil bed. These included (a) no cavity, (b) a stable cavity in the vicinity of the jet, (c) an unstable cavity, and (d) full fluidization. He et al. (2017) developed an analytical model to identify the critical fluidization leakage rate based on the equilibrium of forces and Darcy’s law. The analytical model was used to predict the pore pressure distribution in experiments with different sand-bed heights.

These studies testify to the considerable efforts exerted by researchers to understand the soil fluidization process. However, the limited flexibility in the data acquisition inhibited experimental models from defining crucial parameters for exploring the water-soil interaction, including the soil stresses and liquid pressure inducing soil fluidization. Further research is required to gain a complete understanding of soil behavior and the post-fluidization mechanism.

Soil fluidization around a leaking pipe has also been studied using different numerical approaches. Zhu et al. (2018) adopted two-dimensional Finite Element (FE) models to investigate the effect of varying leakage pressure, crack size and location, and soil layering on the flow regime. However, the initiation of the soil fluidization is associated with a localized cavity formation in the vicinity of the orifice that is characterized by the localization of large strains and large soil displacements. The localized large deformations characteristic from this problem inhibit FE method from simulating the whole fluidization process due to the mesh tangling (Wang et al. 2015). To overcome these drawbacks, Cui et al. (2012) used a coupled Discrete Element Method-Lattice Boltzmann Method (DEM-LBM) to investigate the inhomogeneities of granular particle behavior in the soil fluidization induced by a leaking pipe. DEM is ideal for studying micro-mechanical particulate soil behavior, but it becomes computationally too expensive for real-scale pipe leakage problems.

Considerable effort has been deployed to study the discharge coefficient, the flow regime, the leakage pressure relationship, the pipe material, and the impact of the orifice type and shape on the leakage rate. However, limited studies focused on the effect of orifice size, soil properties, and bed height on the pipe leakage problem. The fluidization mechanism induced by leakage makes them vulnerable parameters. In some cases, soil parameters and bed geometry can be resistance to fluidization. Therefore, investigating the parameters involved in soil fluidization phenomenon helps in identifying the critical state that causes the ground subsidence.

In this study, the Material Point Method (MPM) (Sulsky et al. 1994) is proposed for studying the soil fluidization around leaking pressurized pipes. MPM has proved to be a powerful method in various geotechnical and hydraulic problems, such as the study of granular flow (Więckowski 2003; Yerro et al. 2014; Phuong et al. 2014). MPM is capable of simulating large deformations in multi-material and multi-phase problems (Bandara and Soga 2015). In this method, the continuum is represented by a set of material points (MPs) that act as integration points, which move attached to the media, carrying all the material properties, including e.g., mass, stresses, strains, and displacements. The main governing equations, generally related to dynamic momentum balance, are computed at the nodes of a computational mesh that covers the whole computational domain. The solid-fluid (two-phase) interaction in saturated porous media can be modeled using the two-phase double-point MPM approach (DP) that consists of two sets of MPs (Bandara 2013; Abe et al. 2013; Martinelli 2016; Cao and Neilsen 2021).

This paper uses the DP approach to capture the initiation and evolution of soil fluidization induced by a leaking pipe. Advanced in/outflow Boundary Conditions (BCs) are employed to prescribe velocity-controlled inflow of material points (MPs) into the domain. An advantage of the method adopted here is that it is capable of capturing the development of soil fluidization around a leaking pipe until it reaches the soil surface. However, to the best of the authors' knowledge, there are no publications investigating the critical leakage velocity inducing surface fluidization although there are some useful relationships to identify the onset of soil fluidization. The document is organized as follows. First, the basis of the two-phase DP approach is reviewed, followed by a description of the in/outflow BCs for simulating the water inflow to the domain. Then, the MPM pipe leakage model is presented and qualitatively verified against experimental data. This model is then further parametrized to investigate the effects of orifice size, soil-bed height, and soil porosity on the soil fluidization mechanism. All the analyses presented are performed with an in-house version of the open-source Anura3D MPM software (Anura3D 2021).

Two-Phase Double-Point MPM Approach

Concept

The material point method (MPM) has been applied to solve large deformation problems and multi-phase processes in saturated and unsaturated porous media (Abe et al. 2013; Yerro et al. 2015; Zhao and Liang 2016). The solid-fluid (two-phase) interaction in saturated porous media has been simulated using two distinct approaches (Ceccato et al. 2018), two-phase single-point (SP) and two-phase double-point (DP). The SP formulation consists of one set of material points (MPs) (Zabala and Alonso 2011; Jassim et al. 2013). Each MP represents a portion of the saturated media, and it moves together with the solid phase (i.e., Lagrangian description of the soil motion). The information from the liquid phase is also carried by the MPs using an Eulerian approach. This framework usually assumes the validity of Darcy's law; hence it is not valid when liquid flow is very rapid and non-laminar. The SP formulation is also not appropriate when dealing with the interaction between free water and porous water since the first one has no representation in the domain. Contrarily, the DP formulation (Bandara 2013; Abe et al. 2013; Martinelli 2016; Cao and Neilsen 2021) uses two sets of MPs to represent the solid phase and the liquid phase separately; these are so-called solid material points (SMPs) and liquid material points (LMPs). The DP approach takes full advantage of the Lagrangian description for soil and liquid phases (Abe et al. 2013, Martinelli and Rohe 2015). In the DP framework, the volume fractions theory (Truesdell and Toupin 1960) is used to simulate the solid-liquid interaction. This approach automatically assures the mass conservation of both solid and liquid phases (Ceccato et al. 2018). The SMPs and LMPs are used to compute the velocities of the solid skeleton and water independently, and they are allowed to move separately and overlap. The LMPs can denote the free water as well as the pore water. If the SMPs and LMPs coincide in the same element in the computational mesh, the element is understood as saturated material; hence SMPs account for the pore water in the soil skeleton. The mechanical behavior of the dry soil, saturated soil, free water, and pore water can all be captured in the unified DP MPM framework. Both SP and DP formulations are generally integrated explicitly and consider the weakly compressible liquid.

The SP formulation is only applicable to a laminar flow as the drag force considers the validity of Darcy law. In contrast, the drag force implemented in the DP approach accounts for the gradient of the concentration ratio, laminar flow (in low velocity regime) and non-linear flow (in high velocity regime). Therefore, the use of the DP formulation is vital when the flow velocity is high and the spatial variability of concentrations is significant (Ceccato et al. 2018). In addition, an important feature of the DP formulation compared to the SP approach is the capability of capturing the interaction between the porous media and free water. This is an essential aspect in various geotechnical problems, such as erosion, scouring and fluidization. The number of MPs required to discretize the saturated media in the DP formulation is much larger (at least double) compared to the SP approach. This will inevitably impact the computational time.

In the two-phase DP MPM implementation proposed by Martinelli (2016), the transition between the solid-like or liquid-like state of the solid-liquid mixture is distinguished at the element level through a porosity threshold n_{max}. During the fluidization mechanism, when the porosity of the mixture is lower than n_{max}, the reduction in the mean effective stress leads to an increase in porosity. When the inter-granular contact between the soil grains vanishes, the effective stress becomes zero. The mixture fluidizes when the mixture porosity is greater than n_{max}, such that soil grains are substantially separated. It should be stated that, in the case of sedimentation, the spaces between solid particles decrease, resulting in a reduction in porosity. The effective stresses of the solid particles recur if the porosity of the mixture becomes lower than n_{max}, indicating that the solid grains are in contact, causing the state of the mixture to change from a fluidized state to a solid state. In a solid state, the rate of effective stress in solid constituents is estimated using a conventional soil constitutive law. In the solid-water mixture, the liquid behaviour is described using Equation (2).

$$n_L \rho_L \vec{a}_L = \mathrm{div}\,(\bar{\sigma}_L) - \vec{f}_L^{d} + n_L \rho_L \vec{g} \qquad (2)$$

where n_L is the volumetric concentration ratio of the liquid; ρ_L is the densities of the liquid; $\vec{a}_L$ is the accelerations of the liquid; $\bar{\sigma}_L$ is the partial stresses for the liquid phase; $\vec{f}_L^{d}$ is the drag force of liquid; $\vec{g}$ is the gravitational acceleration.

However, in the liquid-like state, the deviatoric part of the stress tensor of the liquid $\sigma_{dev,L}$ is computed using the following Equation (3).

$$\sigma_{\mathrm{dev,L}} = 2\mu_{\mathrm{L}} \frac{D^L \varepsilon_{vol,L}}{Dt} \qquad (3)$$

where μ_L is the liquid viscosity that considers the solid concentration ratio of the mixture; $\varepsilon_{vol,L}$ is the volumetric strain of the liquid. The deviatoric stress tensor of liquid is set to zero in the case of a solid-like response.

When the mixture porosity is lower than the porosity threshold, the defined granular constitutive model is used to describe the solid-like response of the material (SMPs), which is controlled by the effective stresses. When the mixture porosity exceeds the maximum soil porosity (i.e., critical porosity), the effective stresses in the SMPs become zero, and the liquid-like behavior of the mixture is described using the Navier-Stokes equation (Martinelli et al. 2017). In this process, the constitutive behavior of the material is a Newtonian fluid, which is controlled by an equivalent viscosity that depends on the volumetric concentration ratio of the solid material within the saturated mixture (Beenakker 1984). The equivalent viscosity μ_{eq} is determined using the following Equation (4).

$$\mu_{eq}^{t} = 1 + \frac{5}{2}\tilde{n}_{S,el}^{L,t} + 5.2\,(\tilde{n}_{S,el}^{L,t})^2 \qquad (4)$$

where $\tilde{n}_{S,el}^{L}$ represents the interpolated element solid concentration ratio.

Very recently, the authors of this paper presented a preliminary analysis in which the soil fluidization mechanism due to a leak from a pressurized water pipe was investigated using MPM (Monzer et al. 2022). In this study, the capabilities of both SP and DP approaches are evaluated to simulate the onset and evolution of soil fluidization. It is concluded that the SP formulation is limited to identifying the initiation of the local fluidization due to (a) the inability of the constitutive model to represent the transition from solid-like to liquid-like behavior and (b) the complexity of maintaining an inflow boundary condition when a cavity is formed in the vicinity of the leak.

It is important to note that the use of a damage parameter to gradually transition from a solid to a liquid response, rather than a sudden transition based on a porosity threshold, would be more effective in modelling the behaviour of porous materials. However, the accurate implementation of a damage parameter is a complex task that requires a good understanding of the material behaviour and constitutive models. It is important to calibrate the damage parameter based on experimental data to ensure that it is accurately predicting the behaviour of the material. The accuracy of the sudden transition between solid to liquid by a porosity threshold depends on the specific application and the assumptions made in the model. Although the abrupt transition assumes that the material's properties change abruptly at this threshold, the implemented formulation may provide a reasonable approximation for certain types of porous materials, such as granular soils, which exhibit a sudden change in behaviour at a specific porosity threshold. Additionally, the choice of porosity threshold is based on experimental data, and it is difficult to find a good correlation between the porosity threshold and the damage parameter that can be affected by the material properties. In any case, the implementation of advanced constitutive models in conjunction with the damage parameter is required to provide a robust and realistic representation of the material's behaviour during the fluidization process.

In/Outflow Boundary Condition

For the numerical study of soil response under pressurized leaking pipes, it is necessary to account for inflow and outflow BCs that can ensure consistent water flow through the orifice and a constant water head at the ground surface, respectively. The in/outflow boundary conditions (BCs) developed by Zhao et al. (2019) have been used here as a basis to model BCs. In this analysis, the inflow and outflow zones are attached to the original model (Fig. 1a and 1b) to allow LMPs to enter and leave the computational domain. In the inflow region (Fig. 1a, in green), a constant velocity is prescribed to the LMPs. A zero acceleration is prescribed at the inflow nodes that are shared with the regular elements of the computational region to maintain the imposed velocity field at the boundary, applied to the computation of the governing equation. When an inflow element becomes empty, new LMPs are introduced at the Gauss point locations to refill the inflow elements. In the outflow element (Fig. 1b, in red), the LMPs that enter the outflow elements are consistently removed and a zero pressure is defined at the water surface. The nodes shared by the outflow elements with the computational region have a constant pressure (zero) boundary condition. In other MPM works, the water flow is modeled using a large water reservoir (e.g., Bolognin et al. 2017; Martinelli et al. 2017). However, the water level decreases as water flows throughout the model leading to a progressive drop of the total head at the inflow boundary. The implementation of the in/outflow BCs enables the modeling of constant velocity flows and optimizes the computational cost by simplifying the geometry and reducing the number of MPs.

Numerical Model

The purpose of this numerical analysis is to simulate the soil fluidization induced by a leaking pipe using the two-phase DP MPM approach. The simulated problem is adapted from the experiments conducted by Alsaydalani (2010). The two-dimensional model is shown in Fig. 2, where a saturated homogeneous soil bed is connected to an inlet pipe through an orifice. The soil bed is 300 mm in height and 1500 mm in length. The length of the modeled soil bed is 2.5 times larger than the previous experimental study to avoid BC effects during the evolution of fluidization. A sensitivity analysis was conducted to examine the effect of the length of the soil bed on solution accuracy. Therefore, a careful increase of the bed length was necessary to minimize the numerical noise reflected from the BC. An orifice with a size of 10 mm is located in the middle of the soil base. As the focus of this study at this stage is to investigate the soil behavior around the leaking pipe, only the orifice is modeled and not the whole pipe. Note that the width of the smallest modeled orifice is 2.5 mm, which is 7 times larger than previous experimental and numerical studies (Alsaydalani 2010; Cui 2013). The smaller the orifice, the finer the mesh required to discretize the domain, and the computational cost increases. For instance, the physical time for simulation for a model with an orifice (5 mm) is compared to that of the largest orifice (15 mm) using an Intel Core i7 at 2.50 GHz CPU with 8 GB RAM. The model with a 5 mm orifice consists of 5,153 linear triangular non-structured elements; where the minimum element size is 0.00125 m and increases towards the edges of the model up to 0.033m. On the other hand, the model with a 15 mm orifice consists of 2,415 elements ranging from 0.00375 m to 0.033 m. The computational time decreases by 94% from 162 hour to 10 hour, when changing the orifice size from 5 mm to 15 mm. A parametric analysis is presented in the results section to study the effects of the orifice size.

The water flow is injected through the orifice by applying an upward constant fluid flow at the inflow BC. In the inflow elements (Fig. 2, in green), a prescribed velocity (v_i) is assigned to the LMPs. An empty domain, which does not have any MPs, is attached to the bottom of the inflow elements to avoid the effect of the boundary conditions on the inflow elements. At the top of the model, the outflow region (Fig. 2, in pink) defines a constant free water table consistent with the experiment from Alsaydalani (2010) by removing those LMPs that enter the outflow elements. Free water zones (Fig. 2, in blue) include those elements initially filled with only LMPs. The saturated soil domain (Fig. 2, in light brown) is initialized by placing both SMPs and LMPs to represent the saturated medium. The model consists of 4,753 linear triangular non-structured elements. The mesh is refined around the orifice to better capture the size of the crack and the inflow process. The minimum element size is 0.0025 m and increases towards the edges of the model up to 0.033 m. A parametric analysis to study the influence of the element size at the orifice on the results is presented in the next section. Six MPs per element (three LMPs and three SMPs) are initially assigned to the saturated soil domain, and six LMPs are assigned to the free water and inflow elements. Mechanical fixities are applied at the boundaries as follows. At all boundaries except for the orifice region, the solid and liquid displacements are constrained in the normal direction and are free in the longitudinal direction. At the orifice region, LMPs are allowed to move vertically. The nodes located at the corners between the base of the soil bed and the inlet pipe are fully fixed. Gradual porosity change is considered at the interface of the saturated soil region and the free water. This transition zone is linearly interpolated across the elements of pure liquid and liquid-solid, so it provides a smooth transition between the two regions.

The soil bed is set to be a fully saturated homogenous layer. A linear elastic-perfectly plastic Mohr-Coulomb constitutive model (MC) is used to model the soil constitutive behavior. Mohr-Coulomb is a simple failure criterion that predicts the shearing behavior of soil and thus the overall soil deformation. The free water is modeled with a Newtonian fluid model, while the porous water is assumed linear elastic. The water bulk modulus considered in the simulation is 50000 kPa which is 40 times lower than the real one to increase the critical time step and optimize the computational time with the explicit MPM integration scheme. This does not have a significant influence on the results as it is still considerably larger than the effective bulk modulus of the solid matrix. In order to analyse the effect of water bulk modulus, the original model is compared with another one with a higher bulk modulus of 100000 kPa (reduced by 20 times). The computational time required to analyse the problem with lower water bulk modulus is 10 hour whereas the one with higher water bulk modulus is 97 hour using the same machine, which is almost 10 times faster simulation. This is due to the fact that the critical time step depends on the bulk modulus of the material; the higher the bulk modulus, the larger the critical time step (Liang, 2010). However, the observed fluidization mechanism in both cases is consistent in terms of the porosity distribution and ground movement. This approach of reducing the water bulk modulus to speed up the simulation has been used previously by Liang (2010) and Martinelli et al. (2017). According to Liang (2010), the increased compressibility of water has marginal impacts on the results as the speed of sound is over ten times greater than the maximum flow speed. In addition, a lower bulk modulus of the water is considered to incorporate the possible inclusion of air, and therefore higher compressibility of the water (Ceccato, 2015). Thus, it is concluded that using a reduced water bulk modulus by a factor of 40 is an acceptable approximation. The detailed soil and water parameters used in the analysis are listed in Table 1, which are based on the experimental study conducted by Alsaydalani (2010).

It is worth mentioning that the DP MPM formulation considered here is consistent with the one proposed by Martinelli (2016), in which the Darcy's law is generalized with a non-linear term (Ergun 1952) to account for laminar and steady flow in high-velocity regime. The soil intrinsic permeability (k) is updated using the Kozeny-Carman formula (Bear 1972) that depends on the solid grain diameter (D_p) and the soil porosity (n). Finally, the maximum soil porosity (n_{max}) that differentiates the solid and liquid states of the mixture is determined based on the provided maximum void ratio from Alsaydalani's (2010). A strain-smoothing algorithm is also applied to reduce the kinematic locking (Al-Kafaji 2013).

The effective stresses are initialized via an earth pressure coefficient at rest (K_0) procedure, and pore pressures are initially hydrostatic. In each simulation, a constant inflow velocity (v_i) is prescribed at the orifice throughout the calculation.

Element size in the orifice

The mechanical boundary conditions or fixities in MPM are generally imposed at the mesh nodes. For the problem analyzed here, special attention needs to be paid to the corners of the orifice (Fig. 3). Due to the boundary conditions of the two nodes located at the corners between the base of the soil bed and the inlet (Fig. 3, red nodes), the mobility of the MPs located in the neighboring elements is restricted by this boundary condition (zone of influence of corner nodes). In particular, if an LMP moving vertically from the inflow zone with a prescribed inflow velocity (v_i) enters an element containing one of the corner nodes; it will artificially slow down. This means that v_i is not fully transmitted to the soil. The comparison of the two figures (Fig. 3a and 3b) illustrates that the smaller the elements in the orifice, the smaller the zone of influence restricted by the corner nodes (Fig. 3b).

In order to further understand the effect of the zone of influence of the corner boundaries in the inflow liquid velocity (v_i), a parametric analysis is performed, varying the number of elements at the orifice between one to ten elements. In this analysis, the LMPs are prescribed with three different inflow velocities (v_i) of $0.02, 0.04,$ and $0.10\ m/s$ through a 10 mm orifice. The mesh dependency for the ratio of the transmitted water velocity at the orifice (v_o) with respect to the inflow velocity (v_i) at the inflow BC is shown in Fig. 4. In the simulated problem, the energy losses through the orifice are not considered. Thus, the flow velocity at the orifice (v_o) is expected to be equal to the applied inflow velocity (v_i). The water velocity at the orifice (v_o) is measured by averaging the velocity of the material points passing the orifice region. The ratio of the transmitted water velocity is only 0.4 if one element is considered at the orifice. The ratio increases rapidly from 0.4 to 0.9 when the number of elements increases up to four. Beyond these values, an approximately steady state of the ratio of the transmitted water velocity is observed. Consistent results are obtained for the different prescribed inflow velocities. Therefore, the mesh dependency minimizes as the mesh is refined with the better transmission of the water velocity. Increasing the number of elements beyond four does not significantly improve the results, but it does increase the computational cost. To optimize the computational time while having reasonable results, all models presented herein consider four elements at the orifice.

Results and Discussion

The results obtained with the two-phase DP MPM approach are presented below. First, the soil fluidization mechanism for a reference scenario is discussed. Then, the effects of orifice size, soil-bed height, and soil porosity on the soil fluidization process are investigated through parametric analyses.

Soil Fluidization Mechanism

Soil fluidization initiates when the drag forces exerted by an upward fluid balances the gravitational forces of the bed. This process loosens the soil packing and thus increases the porosity of the material. In this paper, by using the double-point (DP) MPM approach, the transition between solid-like and the liquid-like response of the soil is based on the porosity threshold value n_{max} ; $n < n_{max}$ soil has a solid-like behavior while $n \geq n_{max}$ soil is fluidized. Therefore, tracking the evolution of porosity in the soil mass (SMPs) is a straightforward way to represent the soil state in the model.

A set of numerical models subjected to different inlet velocities through a 10 mm orifice are simulated to investigate the onset and development of soil fluidization mechanism. The porosity distribution at different inlet velocities after 2s of simulation through the centerline of the soil bed is plotted in Fig. 5a. It is observed that the soil porosity increases with the increase in the inflow velocity (v_i) and increases faster in those points located closer to the orifice (i.e., 0.05 m above the orifice). The maximum soil porosity ($n_{max} = 0.50$) corresponds to the critical porosity; hence, $n < n_{max}$ indicates solid-like behavior and $n \geq n_{max}$ indicates fluidized material. When v_i increases from $0.002\, m/s$ to $0.020\, m/s$, the soil porosity immediately above the orifice exceeds (for the first time) the maximum porosity, indicating that fluidization initiates at the orifice. The porosity across the bed height remains essentially constant and equal to the initial value of 0.45. As v_i increases, the fluidized zone expands and develops upward through the soil bed. When v_i reaches to $0.040\, m/s$, the first point situated above the orifice ($0.05\, m$) reaches the critical porosity, which is considered the onset of soil fluidization in the vicinity of the orifice (i.e., onset or initiation of soil fluidization of the soil bed).

At the initiation of soil fluidization, the particles above the orifice are mobilized and moved with the leaking water. This was identified by Alsaydalani (2010) as an 'internally fluidised zone' where the soil within this region was uplifted while those outside the region remained steady (Fig. 6a). The development of the internally fluidized zone is presented in Fig. 6c and 6e. Similarly, Fig. 6b shows the distribution of the porosity after 2s of the MPM simulation across the whole domain for $v_i = 0.04\, m/s$; the fluidized zone localized around the orifice is clearly distinguished in red. The fluidized zone developed with the increase in the inflow velocity (Fig. 6d and 6f). Finally, when the v_i increases up to $0.10\, m/s$, the fluidized zone reaches the ground level (i.e., surface fluidization). Fig. 6g shows how the fluidized region extends from the orifice to the ground surface. The LMPs flow along the ground surface and are consequently dragged away from the fluidized zone.

The inflow velocity required for the initiation of soil fluidization is identified by monitoring the soil bed expansion ratio, which is the ratio between the final soil-bed height H and the initial bed height H_0 (Taghipour et al. 2005). The soil fluidization initiates when the expansion ratio exceeds a value of one resulting in a significant heave of the bed (Chen et al. 2011). The heaving of the soil bed occurs when the upward drag force applied by the water overcomes the bulk weight of the soil. In the numerical model, the soil bed expansion starts when v_i = $0.040\ m/s$, as noticed in Fig. 7, which is in good agreement with the porosity results. The soil bed heaves significantly (10%) by the time the fluidization reaches the surface at an inflow velocity of $0.10\ m/s$.

The soil fluidization mechanism is associated with the uplift of the granular materials above the orifice as was recognized by Alsaydalani (2010) in Figure 8a. The vertical soil displacement for v_i = $0.040\ m/s$ based on the MPM simulation is presented in Fig. 8b; displacements are relatively small (maximum of $1.0\ m$) in the vicinity of the orifice at the onset of fluidization. The MPM prediction is consistent with the experimental result by Alsaydalani (2010). It is worth mentioning that Alsaydalani (2010) assessed the effect of orifice size on the onset of the soil fluidization mechanism. It was concluded that the fluidization zone is not influenced by orifice size for the tested conditions. The inclination angle of the mobilized zone measured from the MPM result is in the order of 63° (Fig. 8b), which is consistent with Alsaydalani's experiment (2010) that used the same soil properties (Fig. 8a). Furthermore, the obtained angle is expected theoretically based on the angle of shear failure that depends on the angle of friction of the soil (34°), i.e. $[\ 45° + \frac{34}{2}] = 62°$. The soil displacements increase as the fluidization reaches the soil surface to $10\ m$ at an inlet velocity of $0.10\ m/s$ (Fig. 8c). The uplift mechanism in the soil bed occurs where the soil is lifted in an upward direction above the orifice leading to the formation of the fluidized zone. Previous researchers (Zoueshtiagh and Merlen 2007; Montellà et al. 2016) have described the significant uplift as a chimney, which is a narrow zone of upward movement of water and soil. The upward progression of the fluidized region results in the entire erosion and instability of the soil in the chimney. Overall, these results qualitatively validate the observations from previous experimental results.

The fluidization mechanism is also attributed to an abrupt drop in the effective stress where the contact forces between the grains vanish. The effective stress at different inflow velocities through the centerline of the soil bed is plotted in Fig. 9 after 2s of simulation. It is found that the effective stress decreases with the increase in the inflow velocity ($\mathrm{v_i}$) and drops faster at the vicinity of the orifice. When $\mathrm{v_i}$ increases from $0.002\ \mathrm{m/s}$ to $0.040\ \mathrm{m/s}$, the effective stress at 0.05 m above the orifice decreases to zero, indicating the onset of the soil fluidization at which the leakage force exerted by the upward flow balances the bulk weight of the soil. When the $\mathrm{v_i}$ increases, up to $0.10\ \mathrm{m/s}$, the effective stress across the bed height becomes null where the fluidization reaches the ground surface. It is worth noting that this study focuses on the initiation and progression of the fluidization mechanism up to the ground surface. Once the fluidized zone reaches the bed surface, the simulation becomes unstable, and the post-fluidization mechanism (i.e., behavior after the fluidization reaches the ground surface) cannot be analyzed. One explanation for the numerical instabilities is that the two-phase DP MPM approach used here considers the liquid as weakly compressible, which can generate pressure oscillations when simulating nearly incompressible pressurized flows (Kularathna and Soga 2017; Yamaguchi et al. 2020; Zhao and Choo 2020; Kularathna et al. 2021; Sołowski et al. 2021).

Parametric Study

Effect of Orifice Size

Five simulations with different orifice sizes (2.5, 5.0, 7.5, 10.0, 12.5, and 15.0 mm) are conducted to investigate the effect of orifice size on the soil fluidization process induced by a leaking pressurized water pipe. The numerical results of the porosity at different inflow velocities through the centerline of the soil bed for different orifice sizes (o) are plotted in Fig. 10. Consistently with the results presented in the previous section, the onset of soil fluidization is determined when the SMPs at 0.05 m above the orifice fluidizes ($n \geq n_{max}$), while surface fluidization is determined when all SMPs through the centerline of the soil bed are fluidized ($n \geq n_{max}$). The inflow required for the onset (v_{io}) and surface fluidization (v_{is}) in models with different orifice sizes are presented in Fig. 11. The vertical lines represent the accuracy of the inflow velocity that are calculated based on ranges of values of soil porosity (Fig. 10). It is observed that the inflow velocity inducing the onset of the soil fluidization (v_{io}) decreases with an increase in the orifice size. As the orifice size increases from 5 mm to 15 mm, v_{io} decreases from $0.08\ m/s$ to $0.02\ m/s$. It is of interest to note that the inflow flow rate is a function of orifice area multiplied by the inflow velocities. The critical flow rate to initiate soil fluidization decreases considerably from $1440\ l/h$ to $1080\ l/h$, corresponding to an orifice size of 5 mm and 15 mm, respectively. The inflow velocity inducing the surface fluidization (v_{is}) decreases from $0.16\ m/s$ to $0.08\ m/s$ as the orifice size increases from 5 mm to 15 mm. Therefore, the larger the orifice size, the smaller are the inflow velocities required to trigger the onset and surface fluidization. These results are consistent with the analytical predictions developed by Tang et al. (2017) in their study for the sand erosion caused by an upward water jet. If the orifice is large enough, the soil fluidization progresses rapidly and reaches the surface at minimal leakage velocity. In contrast, smaller orifices provide less water flow to fluidize the soil bed.

The range of orifice sizes considered in this study is at least 7 times larger than the experimental study used for reference (Alsaydalani 2010), which used o = 0.336 mm. This is selected to reduce the computational cost of the models and avoid numerical instabilities as smaller orifice requires finer mesh to discretize the domain. From the numerical results, a second-order polynomial trendline for the inflow required for the onset of soil fluidization (v_{io}) is plotted in Fig. 11. This trendline is represented using the following Equation (5).

$$v_{io} = 0.0003o^2 - 0.0126o + 0.1345 \qquad (5)$$

where v_{io} is in m/s, and o is the orifice size in mm. Note that Equation (4) is specific for the material properties and soil bed heigh considered in the MPM model, which are consistent with Alsaydalani (2010), and it is not a generic expression. The experimental results from Alsaydalani (2010) indicate that $v_{io} = 0.12\, m/s$ was required to initiate soil fluidization through a 0.336 mm orifice. This value is derived after deducting the velocity loss measured through the orifice. Based on Equation (1), the predicted inflow velocity causing the initiation of soil fluidization (v_{io}) for an orifice size of 0.336 mm is $0.13\, m/s$ (Fig. 11), which is very similar to the experimental results. This exercise further validates the consistency of the model with the available data.

The change in expansion ratio H/H_0 with the inflow velocity for different orifice sizes is presented in Fig. 12. The larger orifice size results in more heaving of the soil bed at the same inflow velocity. This agrees well with the experiment conducted by Weisman and Lennon (1994) in the development of fluidizer systems. As the orifice size increased, the soil fluidization occurred rapidly at minimal leakage velocity. An increase in the orifice opening leads to a lower expansion ratio at the onset of fluidization. The final expansion ratio as the fluidization reaches the ground level is not significantly affected by the orifice size. Therefore, the orifice size mainly affects the initiation of the soil fluidization process.

Effect of Soil-Bed Height

Five numerical models with different soil-bed heights are simulated to explore the effect of bed height on the soil fluidization mechanism. To eliminate the effect of boundary conditions on the fluidization zone, the ratio Length/Height of the soil bed is kept constant for the different simulations. Thus, four simulations with different bed heights of 300, 400, 500, 600, and 700 mm are conducted with a soil-bed length of 1500, 2000, 2500, 3000, and 3500 mm, respectively. Fig. 13 shows the change in the inflow velocity needed for the onset (v_{io}) and surface (v_{is}) fluidization at a 10 mm orifice with the change of the bed height. In the presented example, the inflow velocity leading to the initiation of the soil fluidization (v_{io}) increases with an increase in the soil bed height. As the bed height increases from 300 mm to 700 mm, v_{io} increases from $0.04\ m/s$ to $0.10\ m/s$. Similarly, the water velocity at the orifice required to observe surface fluidization (v_{is}) increases considerably from $0.10\ m/s$ to $0.40\ m/s$, corresponding to a bed height of 300 mm and 700 mm, respectively. Thus, the velocity required to induce surface fluidization significantly increases with the bed height.

The variation in the expansion ratio H/H_0 with the inflow velocity is plotted for different bed heights in Fig. 14. The thicker the soil-bed, the lower the expansion ratio H/H_0 at the same inflow velocity. As the height of the soil bed increases, higher leakage velocity is required to initiate soil fluidization. The effect of the soil-bed height is not significant in terms of the expansion ratio at the onset of fluidization. However, the thicker the soil-bed height results in a lower expansion ratio when the fluidization reaches the surface. This agrees with the previous study conducted by Tang et al. (2017) that concluded the thicker soil bed is characterized by more resistance of the mobilized soil region. Therefore, a larger inflow velocity is required to fluidize the above soil bed.

Effect of Soil Porosity

To explore the effects of the soil porosity on soil fluidization induced by a leaking pipe, models with four different initial soil porosity (0.30, 0.35, 0.40, and 0.45) have been conducted. In the simulated problem, the intrinsic soil permeability (k) depends on the solid grain diameter (D_p) and the soil porosity (n) (Bear 1972). Alsaydalani and Clayton (2013) stated that permeability, and therefore soil porosity, can be expected to have a large effect on the water flowing into the soil bed. Water seepage in the soil bed with higher porosity will be easily dissipated, which can quickly induce soil bed fluidization at the lower inflow velocity. For example, an inflow velocity (v_{io}) of $0.10\ m/s$ at a 10 mm orifice in a soil bed with 0.30 initial porosity is sufficient to initiate the soil fluidization (Fig. 15a). For higher soil porosity (0.45), the soil fluidization is initiated at a lower inflow velocity (v_{io}) of $0.04\ m/s$. Soil fluidization initiates under a lower inflow velocity in a higher porosity soil bed. Similarly, the inflow velocity (v_{is}) required to develop fluidization reaching the bed surface decreases with an increase in the soil porosity. The inflow velocity inducing the surface fluidization (v_{is}) decreases from $0.16\ m/s$ to $0.10\ m/s$ as the soil porosity increases from 0.30 (Fig. 15b) to 0.45 (Fig. 15e). Thus, the inflow velocity required for the onset (v_{io}) and surface (v_{is}) fluidization decreases linearly with the increase of the soil porosity. Hence, soil porosity is an essential parameter in soil fluidization, and lowering the soil porosity can effectively improve the stability of the soil bed.

The effect of porosity on the surface heaving at the onset of fluidization is also studied. Fig. 16a shows the change in soil-height expansion ratio as the inflow velocity increases in the soil bed with different initial soil porosity. The inflow velocity that induces soil fluidization (v_{io}) is determined when the soil bed expansion ratio H/H_0 exceeds one. Water can easily flow through the soil when the soil porosity is large, and soil-bed fluidization is initiated at a lower inflow velocity, as shown in Fig. 16a. This higher water velocity results in an increase in the expansion ratio. On the other hand, flow is more difficult through the lower porosity soil because of the lower permeability. The higher the porosity of the soil-bed, the lower the expansion ratio at the same leakage velocity. The expansion ratio is lower as the soil fluidization reaches the surface in highly porous soil. Fig. 16b and Fig. 16c show the vertical soil displacement as the fluidization reaches the soil surface in soil bed with an initial soil porosity of 0.30 and 0.35, respectively. The soil vertical displacements in lower porous soil are relatively high (maximum of $0.06\ m$) compared to the vertical displacements that occurred in highly porous soil (maximum of $0.05\ m$). Chen et al. (2011) stated that the driving force exerted by the water to the solid skeleton decreases as the soil porosity increases, and this decrease in driving force makes the soil bed more difficult to heave.

Summary and Conclusions

In this study, the onset and development of soil fluidization induced by a leaking pressurized water pipe embedded in fully saturated soil are simulated using the two-phase double-point MPM approach, together with the use of in/outflow boundary conditions. This formulation captures the transition from solid to liquid behavior resulting from the fluidization mechanism considering a threshold porosity; beyond that value, the material is considered a Newtonian fluid. The MPM results capture the initiation and evolution of soil fluidization and soil bed expansion changes during the infiltration process. As the leakage velocity increases, the soil porosity close to the orifice increases until it exceeds the maximum porosity at the onset of fluidization. Soil fluidization results in a significant soil bed expansion that increases with the propagation of the fluidized zone. Based on this analysis, an equation is proposed to predict the inflow velocity at which fluidization starts to verify the numerical model against previous experimental works. The MPM model is used to investigate the impacts of the orifice size, soil bed height, and soil porosity on the soil fluidization mechanism around a leaking pipe. Based on the numerical simulations, the following conclusions can be made:

- An increase in orifice size can considerably decrease the inflow velocity resulting in soil fluidization. The surface fluidization mechanism is not significantly affected by the orifice size.
- The inflow leakage velocity required for the onset and evolution of soil fluidization significantly increases with an increase in the soil-bed height. The effect of the soil-bed height is more than the effect of orifice size, which means that it will be more effective to increase the pipe burial depth to reduce fluidization risk; and
- The soil porosity is an essential factor in soil fluidization, and the decrease in soil porosity can effectively strengthen the stability of the soil bed. Thus, soil with lower porosity should be used around underground pipes.

These results contribute to the understanding of the consequences of pipe leakage in pressurized water pipes and help identifying the most important parameters contributing to the initiation and propagation of soil fluidization. It is worth mentioning that further work is needed to address the soil-fluid transition in a more accurate way by means of using advanced constitutive models.

Data Availability Statement

Some or all data, models, or code that support the findings of this study are available from the corresponding author upon reasonable request.

Acknowledgements

The authors extend their appreciation to the school of Engineering at University of Birmingham and Anura3D Research Community for providing the necessary support to complete this research. The authors wish to extend their gratitude to John Murphy in the University of California, Berkeley for his kind guidance in terms of double-point MPM code.

References

Abe, K., Soga, K., and Bandara, S. (2013). “Material Point Method for Coupled Hydromechanical Problems.” *Journal of Geotechnical and Geoenvironmental Engineering,* 140 (3), pp. 1–16.

Al-Kafaji, I. K. J. (2013). "Formulation of a Dynamic Material Point Method (MPM) for Geomechanical Problems." Ph.D. Thesis, Dept. of Civil and Environmental Engineering, Univ. of Stuttgart.

Alsaydalani, M. O. A., and Clayton, C. R. I. (2013). "Internal fluidization in granular soils." *Journal of Geotechnical and Geoenvironmental Engineering,* 140(3), 04013024.

Alsaydalani, M.O.A. (2010). "Internal fluidization of granular material." Ph.D. thesis. Univ. of Southampton.

Anura3D (2021). "Anura3D MPM Research Community." Accessed March 18, 2022. http://www.anura3d.com/.

Awad, A. S., and Karni, A. (2000). "Stability of saturated cohesionless soil layer due to water flowing from a broken underground pipeline." *Journal of King Saud University,* 12 (1), 27-44.

Bandara S. and Soga K. (2015). "Coupling of soil deformation and pore fluid flow using material point method." *Computers and Geotechnics*, 63, 199-214.

Bandara, S. (2013). "Material point method to simulate large deformation problems in fluid-saturated granular medium." Ph.D. Thesis, Univ. of Cambridge.

Bear, J. (1972). *Dynamics of fluids in porous media.* New York: Elsevier.

Beenakker, C.W.J. (1984). "The effective viscosity of a concentrated suspension of spheres (and its relation to diffusion)." *Physica*, 128, 48–81.

Bolognin, M., Martinelli, M., Bakker, K.J., and Jonkman, S.N. (2017). "Validation of material point method for soil fluidisation analysis." *Journal of Hydrodynamics,* 29 (3), 431-437.

Cao, C. and Neilsen, M. (2021). "Dam Breach Simulation with the Material Point Method." *Computation,* 9 (2), 8.

Ceccato, F. (2015). "Study of large deformation geomechanical problems with the material point method." Ph.D. thesis. Universita degli Studi di Padova.

Ceccato, F., Yerro, A. and Martinelli, M. (2018). "Modelling soil-water interaction with the material point method. Evaluation of single-point and double-point formulations." In *Numerical Methods in Geotechnical Engineering IX, Proceedings of the 9th European Conference on Numerical Methods in Geotechnical Engineering,* 25-27 June. Porto, Portugal. CRC Press.

Chen, X.-Z., Shi, D.-P., Gao, X., and Luo, Z.-H. (2011). "A fundamental CFD study of the gas–solid flow field in fluidized bed polymerization reactors." *Powder Technology,* 205 (1-3), 276-288.

Cui, X. (2013). “Numerical simulation of internal fluidization and cavity evolution due to a leaking pipe using the coupled DEM-LBM technique.” Ph.D. Thesis. Univ. of Birmingham.

Cui, X., Li, J., Chan, A., and Chapman, D. (2012). “A 2D DEM–LBM study on soil behaviour due to locally injected fluid.” *Particuology,* 10 (2), 242–252.

Ergun, S. (1952). “Fluid flow through packed columns.” Chem. Eng. Prog. 48, 89-94.

Germanopoulos, G., and Jowitt, P. (1989). “Leakage reduction by excess pressure minimization in a water supply network.” *Proceedings of the Institution of Civil Engineers,* 87, 195-214.

Guo, S., Shao, Y., Zhang, T., Zhu, D. Z., and Zhang, Y. (2013). “Physical modeling on sand erosion around defective sewer pipes under the influence of groundwater.” *Journal of Hydraulic Engineering,* 139 (12), 1247-1257.

He, Y., Zhu, D.Z., Zhang, T., Shao, Y., and Yu, T. (2017). “Experimental observations on the initiation of sand-bed erosion by an upward water jet.” *Journal of Hydraulic Engineering,* 143 (7), 06017007.

Jassim, I., Stolle, D. and Vermeer, P. (2013). “Two-phase dynamic analysis by material point method.” *International journal for numerical and analytical methods in geomechanics,* 37 (15), 2502-2522.

Kingdom, B., Liemberger, R., and Marin, P. (2006). “The Challenge of Reducing Non-Revenue Water (NRW) in Developing Countries.” *Water Supply and Sanitation Board Discussion Series,* The World Bank, Washington DC. USA.

Kularathna, S. and Soga, K. (2017). “Comparison of two projection methods for modeling incompressible flows in MPM.” *Journal of Hydrodynamics,* 29 (3), 405-412.

Kularathna, S., Liang, W., Zhao, T., Chandra, B., Zhao, J., and Soga, K. (2021). “A semi-implicit material point method based on fractional-step method for saturated soil.” *International Journal for Numerical and Analytical Methods in Geomechanics,* 45 (10), 1405-1436.

Lambert, A. (2001). “What do we know about pressure-leakage relationships in distribution systems.” In *IWA Conf. n Systems approach to leakage control and water distribution system management.*

Lennon, G. P., and Weisman, R. N. (1995). “Head requirement for incipient fluidization of fine sands in unbounded domains.” *Journal of Hydraulic Engineering,* 121 (11), 838–841.

Li, J. (2013). “Numerical investigations of the coupled DEM-LBM technique with application to leakage-soil interaction due to a leaking pipe.” Ph.D. Thesis. Univ. of Birmingham.

Liang, D. (2010). “Evaluating shallow water assumptions in dam-break flows.” *In Proceedings of the Institution of Civil Engineers-Water Management,* 163 (5), 227-237.

Martinelli, M. (2016). “Soil-water interaction with material point method. double-point formulation.” *Report on EU-FP7 research project MPM-Dredge PIAP-GA-2012 324522.*

Martinelli, M. and Rohe, A. (2015). “Modelling fluidization and sedimentation using material point method.” *in 1st Pan-American Congress on Computational Mechanics.* Buenos Aires, Argentinia.

Martinelli, M., Rohe, A. and Soga, K. (2017). “Modeling dike failure using the material point method.” *Procedia Engineering,* 175, 341-348.

Martinelli, M., Tehrani, F.S. and Galavi, V. (2017). “Analysis of crater development around damaged pipelines using the material point method.” *Procedia Engineering*, 175, 204-211.

Montellà, E.P., Toraldo, M., Chareyre, B. and Sibille, L. (2016). “Localized fluidization in granular materials: Theoretical and numerical study.” *Physical Review E,* 94 (5), 052905.

Monzer, A., Murphy, J., Yerro, A., Faramarzi, A. and Chapman, D. (2022). “Simulation of Soil Fluidization Around a Pressurized Leaking Pipe Using the Material Point Method.” In *Geo-Congress 2022*, 363-374.

OECD (2016) Water governance in cities. OECD Publishing. Available at: www.read.oecd-ilibrary.org/governance/water-governance-in-cities.com

Phuong, N., van Tol, A., Elkadi, A., and Rohe, A. (2014). “Modelling of pile installation using the material point method (MPM).” *Numerical Methods in Geotechnical Engineering,* 271, 271-276.

Richards Jr, R., Elms, D.G., and Budhu, M. (1990). “Dynamic fluidization of soils.” *Journal of Geotechnical Engineering*, 116 (5), 740-759.

Rogers, D. (2014). “Leaking water networks: an economic and environmental disaster.*” In Proceedings of the 12th International Conference on Computing and Control for the Water Industry,* 70, 1421-1429.

Sołowski, W.T., Berzins, M., Coombs, W.M., Guilkey, J.E., Möller, M., Tran, Q.A., Adibaskoro, T., Seyedan, S., Tielen, R., and Soga, K. (2021). “Material point method: Overview and challenges ahead.” *Advances in Applied Mechanics,* 54, 113-204.

Sulsky, D., Chen, Z., and Schreyer, H.L. (1994). “A particle method for history-dependent materials.” *Computer methods in applied mechanics and engineering*, 118 (1-2), 179-196.

Taghipour, F., Ellis, N., and Wong, C. (2005). “Experimental and computational study of gas-solid fluidized bed hydrodynamics.” *Chemical engineering science,* 60 (24), 6857-6867.

Tang, Y., Zhu, D.Z., and Chan, D.H. (2017). “Experimental study on submerged sand erosion through a slot on a defective pipe.” *Journal of Hydraulic Engineering,* 143 (9), 04017026.

Toshifumi, M., Naoko, K., and Jun, O. (2012). “Image analysis of soil failure on defective underground pipe due to cyclic water supply and drainage using X-ray CT.” *Frontiers of Structural and Civil Engineering,* 6 (2), 85-100.

Truesdell, C., and Toupin, R. (1960). “The classical field theories.” In *Principles of classical mechanics and field theory/Prinzipien der Klassischen Mechanik und Feldtheorie*. Springer, Berlin, Heidelberg.

van Zyl, J.E., and Clayton, C.R.I. (2007). “The effect of pressure on leakage in water distribution systems.” *Proceedings of the Institution of Civil Engineers-Water Management.* Thomas Telford Ltd. 109–114.

van Zyl, J.E., CGeol, F.G.S., and BIng, A.D. (2013). “Soil fluidization outside leaks in water distribution pipes-preliminary observations.” *Proceedings of the Institution of Civil Engineers,* 166 (10), 546.

Walski, T., Bezts, W., Posluszny, E. T., Weir, M., and Whitman, B. E. (2006). “Modeling leakage reduction through pressure control.” *Journal-American Water Works Association,* 98 (4), 147-155.

Waltham, A. (1993). “Crown Hole Development in the Sandstone Caves of Nottingham.” *Quarterly Journal of Engineering Geology and Hydrogeology,* 26, 243-251.

Wang, D., Bienen, B., Nazem, M., Tian, Y., Zheng, J., Pucker, T., and Randolph, M.F. (2015). “Large deformation finite element analyses in geotechnical engineering.” *Computers and Geotechnics*, 65, 104–114.

Weisman, R. N., and Lennon, G. P. (1994). “Design of Fluidiser Systems for Coastal Engineering.” *Journal of Waterway, Port, Coastal, and Ocean Engineering,* 120 (5), 468-487.

Więckowski, Z. (2003). “Modelling of silo discharge and filling problems by the material point method.” *Task Quarterly*, 4 (4), 701-721.

Yamaguchi, Y., Takase, S., Moriguchi, S., and Terada, K. (2020). "Solid-liquid coupled material point method for simulation of ground collapse with fluidization." *Computational Particle Mechanics,* 7 (2), 209-223.

Yerro, A, Alonso, E and Pinyol, N (2014). "Modelling progressive failure with MPM." In *Numerical Methods in Geotechnical Engineering.* Balkema, Leiden. The Netherlands, 319–323.

Yerro, A. (2015) "MPM modelling of landslides in brittle and unsaturated soils." Ph.D. Thesis. Univ. Politècnica de Catalunya.

Zabala, F. and Alonso, E.E. (2011). "Progressive failure of Aznalcóllar dam using the material point method." *Géotechnique*, 61 (9), 795-808.

Zhao, X. and Liang, D. (2016). "MPM modelling of seepage flow through embankments." *Proceedings of the Twenty-Sixth (2016) International Ocean and Polar Engineering Conference.* Rodos, Greece, 1161–1165.

Zhao, X., Bolognin, M., Liang, D., Rohe, A., and Vardon, P.J. (2019). "Development of in/outflow boundary conditions for MPM simulation of uniform and non-uniform open channel flows." *Computers and Fluids,* 179, 27-33.

Zhao, Y., and Choo, J. (2020). "Stabilized material point methods for coupled large deformation and fluid flow in porous materials." *Computer Methods in Applied Mechanics and Engineering,* 362, 112742.

Zhu, H., Zhang, L., Chen, C., and Chan, K. (2018). "Three-dimensional modelling of water flow due to leakage from pressurized buried pipe." *Geomechanics and Engineering,* 16 (4), 423-433.

Zoueshtiagh, F. and Merlen, A. (2007). "Effect of a vertically flowing water jet underneath a granular bed." *Physical review E,* 75 (5), 056313.

Table 1. Material properties of the silica sand and water used in the model (Alsaydalani 2010).

Material Parameter	**Symbol**	**Unit**	**Value**
Initial porosity	n_0	$-$	0.45
Intrinsic permeability	k	m^2	4.0×10^{-11}
Density soil	ρ_s	kg/m^3	2660
Water density	ρ_l	kg/m^3	1000
Water bulk modulus	K_l	kPa	50000
Water viscosity	μ_d	$kPa.s$	10^{-6}
K_0-value	K_0	$-$	0.44
Effective Poisson ratio	v'	$-$	0.3
Effective Young's modulus	E'	kPa	69000
Effective Cohesion	c'	kPa	1.0
Effective friction angle	ϕ'	$degree$	34
Soil grain diameter	D_p	mm	0.9
Maximum soil porosity	n_{max}	$-$	0.50

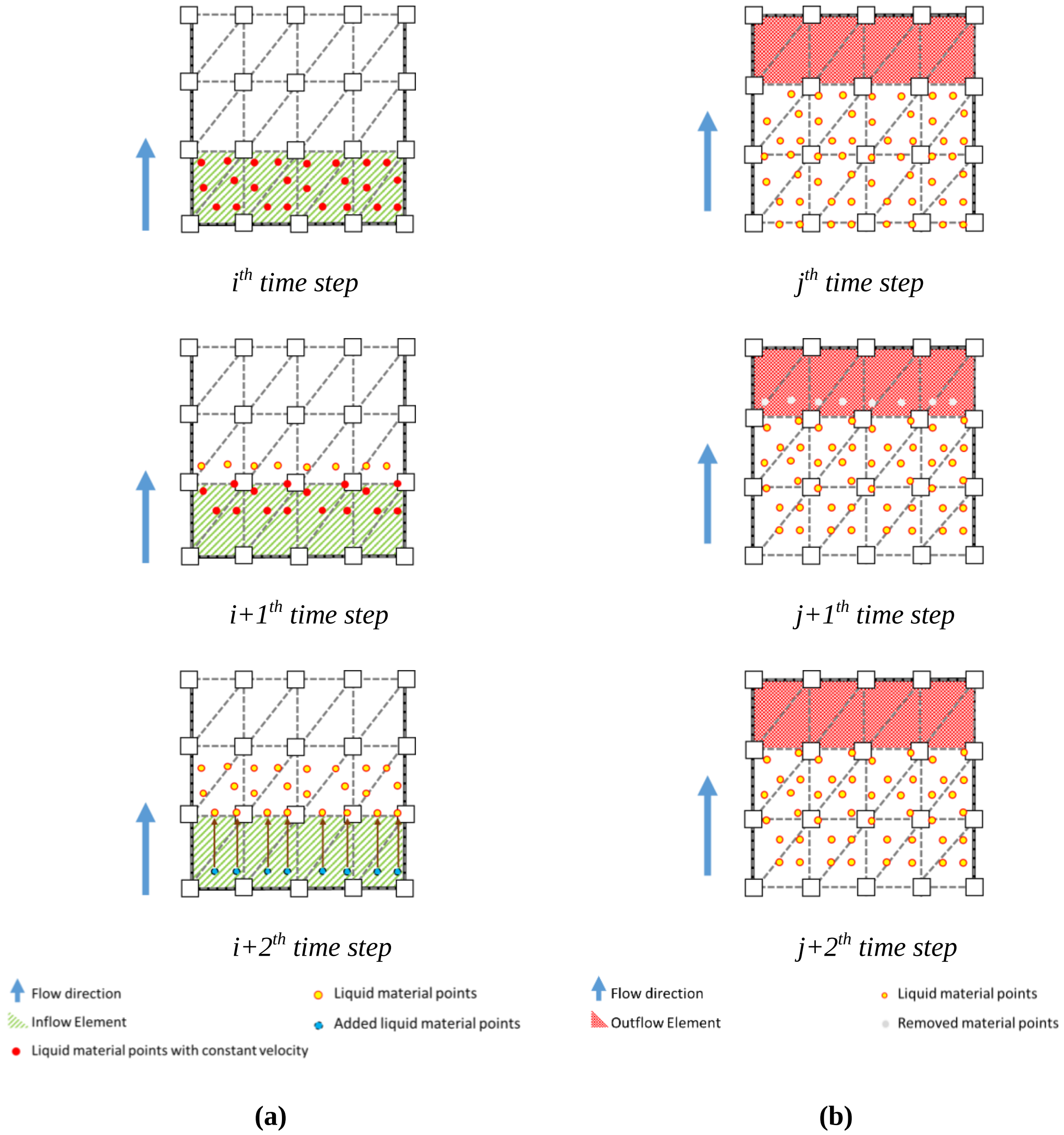

i^th time step
i+1^th time step
i+2^th time step
Flow direction
Inflow Element
Liquid material points with constant velocity
Liquid material points
Added liquid material points
(a)
j^th time step
j+1^th time step
j+2^th time step
Flow direction
Outflow Element
Liquid material points
Removed material points
(b)

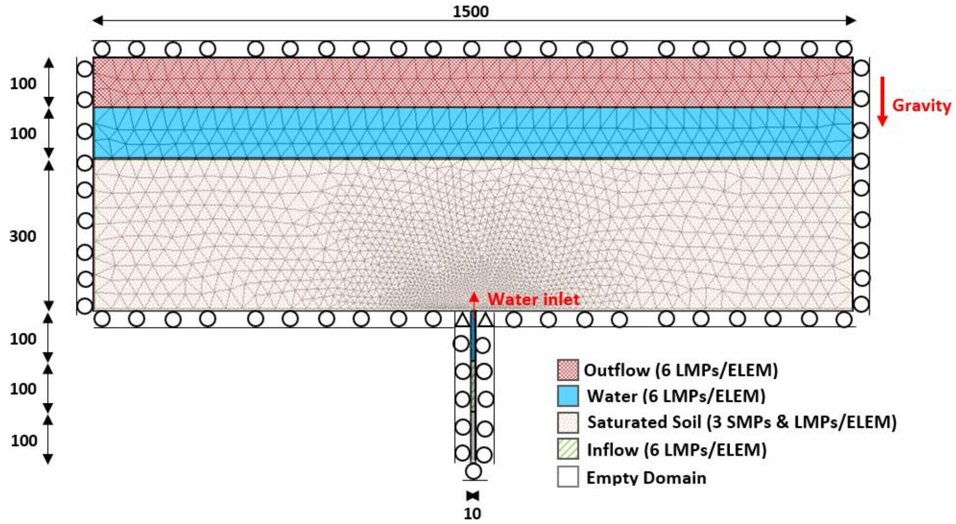

1500
100
100
300
100
100
100
10
Gravity
Water inlet
Outflow (6 LMPs/ELEM)
Water (6 LMPs/ELEM)
Saturated Soil (3 SMPs & LMPs/ELEM)
Inflow (6 LMPs/ELEM)
Empty Domain

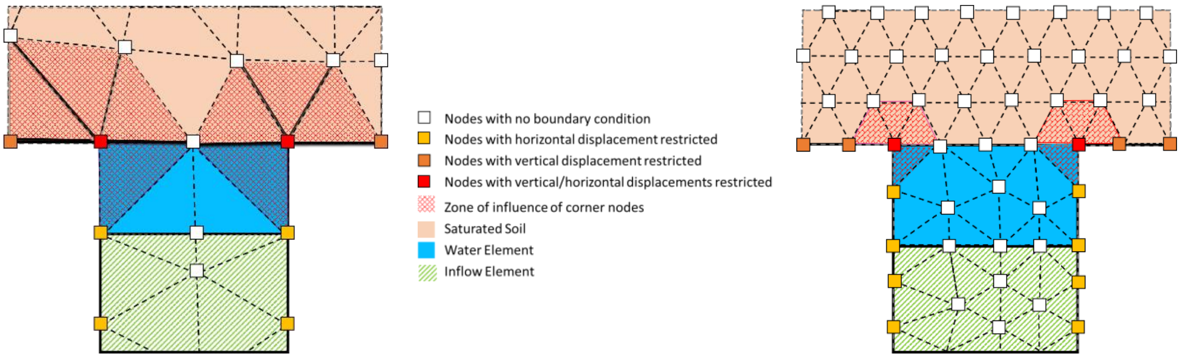
Nodes with no boundary condition
Nodes with horizontal displacement restricted
Nodes with vertical displacement restricted
Nodes with vertical/horizontal displacements restricted
Zone of influence of corner nodes
Saturated Soil
Water Element
Inflow Element

(a) **(b)**

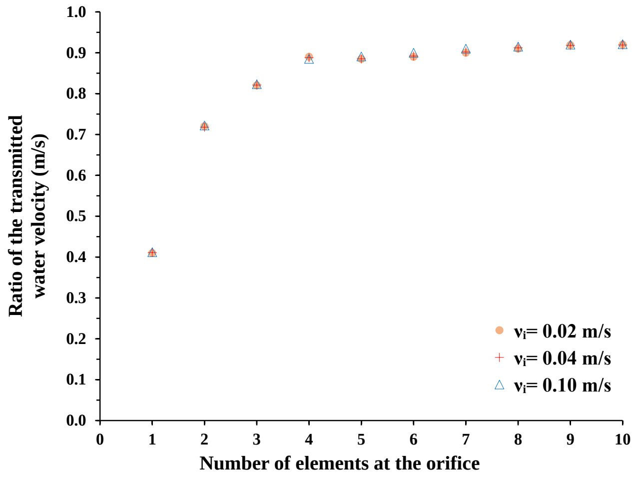

Ratio of the transmitted water velocity (m/s)
1.0
0.9
0.8
0.7
0.6
0.5
0.4
0.3
0.2
0.1
0.0
0
1
2
3
4
5
6
7
8
9
10
Number of elements at the orifice
vi= 0.02 m/s
vi= 0.04 m/s
vi= 0.10 m/s

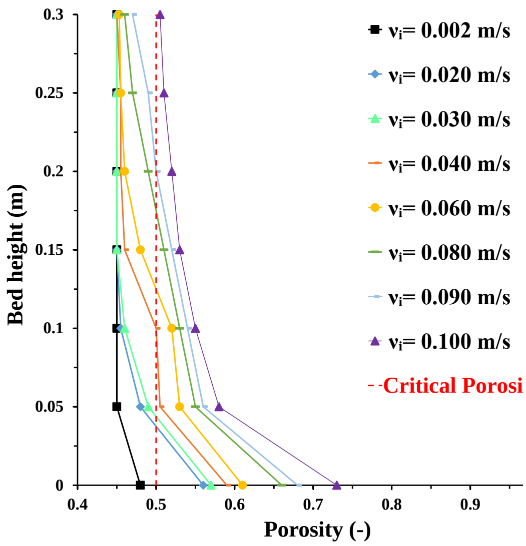

Bed height (m)
0.3
0.25
0.2
0.15
0.1
0.05
0
0.4
0.5
0.6
0.7
0.8
0.9
Porosity (-)
vi= 0.002 m/s
vi= 0.020 m/s
vi= 0.030 m/s
vi= 0.040 m/s
vi= 0.060 m/s
vi= 0.080 m/s
vi= 0.090 m/s
vi= 0.100 m/s
Critical Porosi

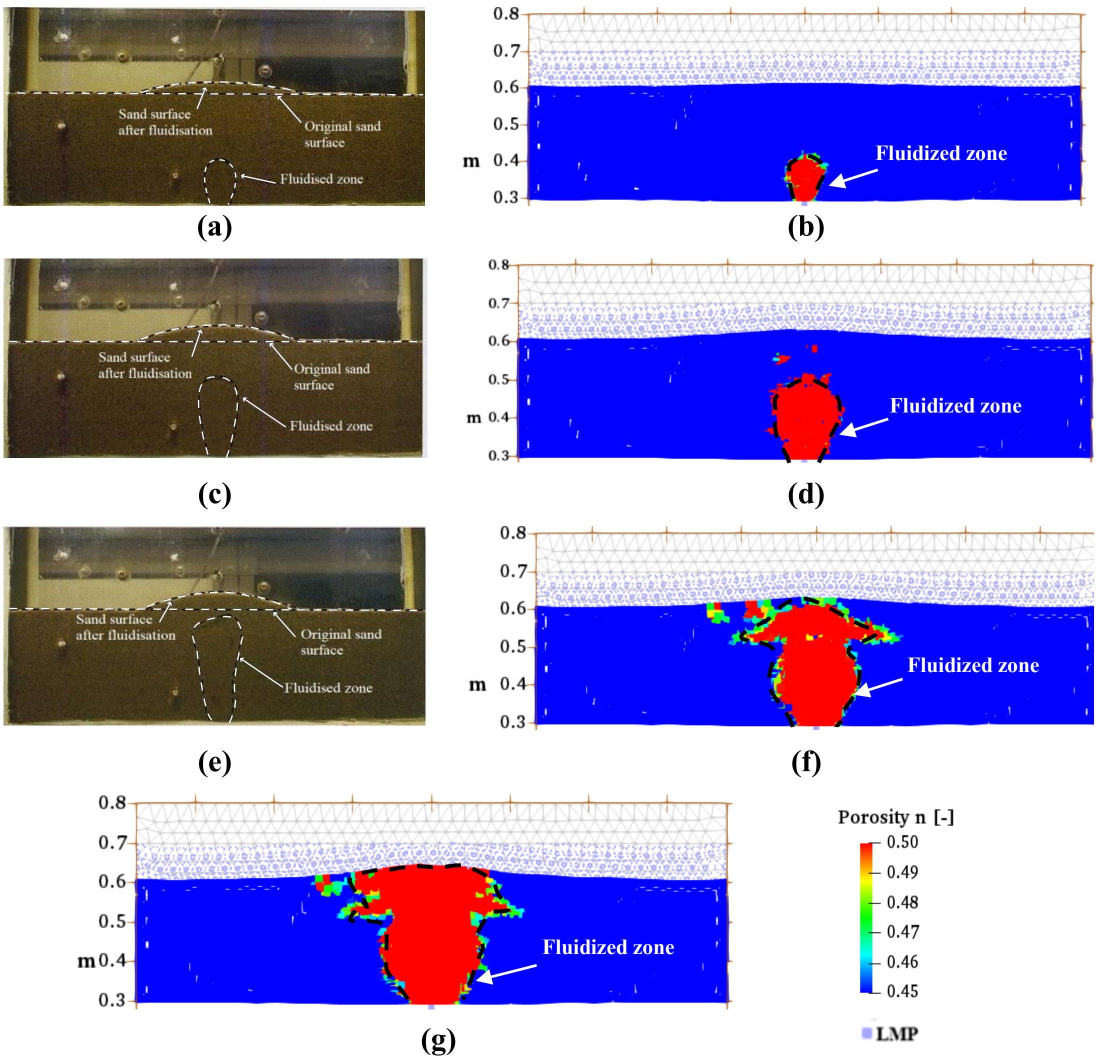
Sand surface
after fluidisation
Original sand
surface
Fluidised zone
(a)
0.8
0.7
0.6
0.5
m 0.4
0.3
Fluidized zone
(b)
(c)
(d)
(e)
(f)
(g)
Porosity n [-]
0.50
0.49
0.48
0.47
0.46
0.45
LMP

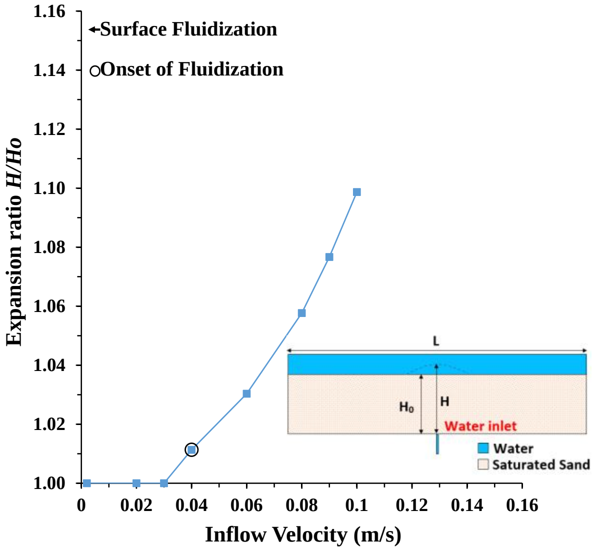

Surface Fluidization
Onset of Fluidization
Expansion ratio H/Ho
1.16
1.14
1.12
1.10
1.08
1.06
1.04
1.02
1.00
0
0.02
0.04
0.06
0.08
0.1
0.12
0.14
0.16
Inflow Velocity (m/s)
L
H0
H
Water inlet
Water
Saturated Sand

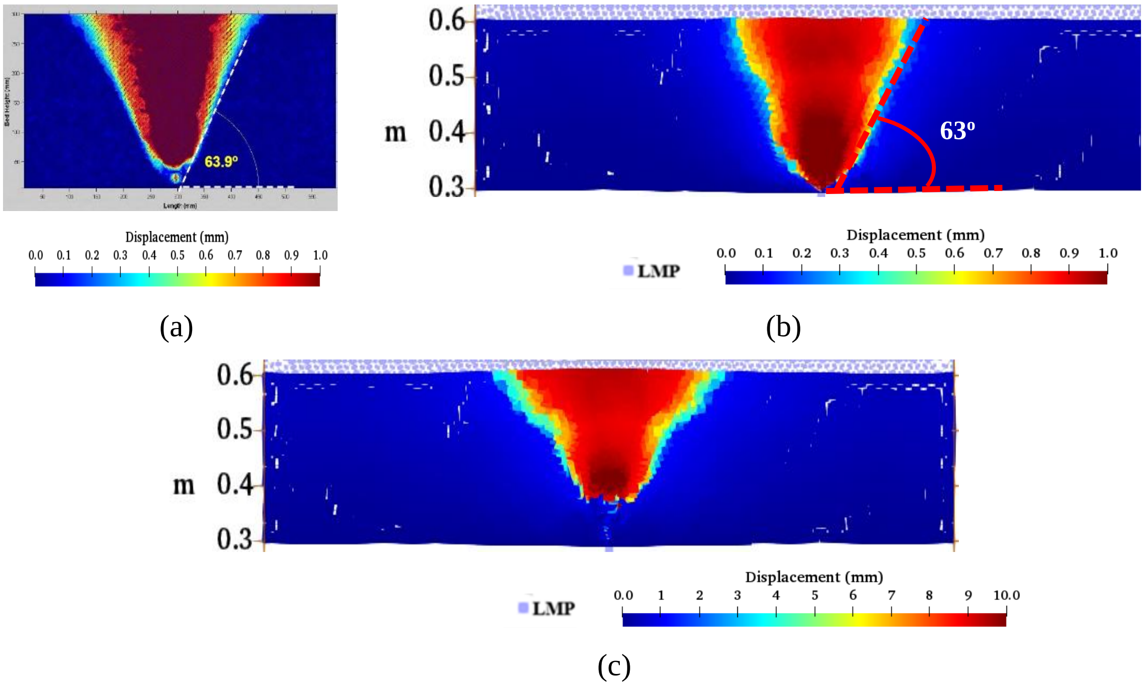
63.9°
Displacement (mm)
0.0 0.1 0.2 0.3 0.4 0.5 0.6 0.7 0.8 0.9 1.0
(a)
0.6
0.5
m 0.4
0.3
63°
Displacement (mm)
LMP
0.0 0.1 0.2 0.3 0.4 0.5 0.6 0.7 0.8 0.9 1.0
(b)
0.6
0.5
m 0.4
0.3
Displacement (mm)
LMP
0.0 1 2 3 4 5 6 7 8 9 10.0
(c)

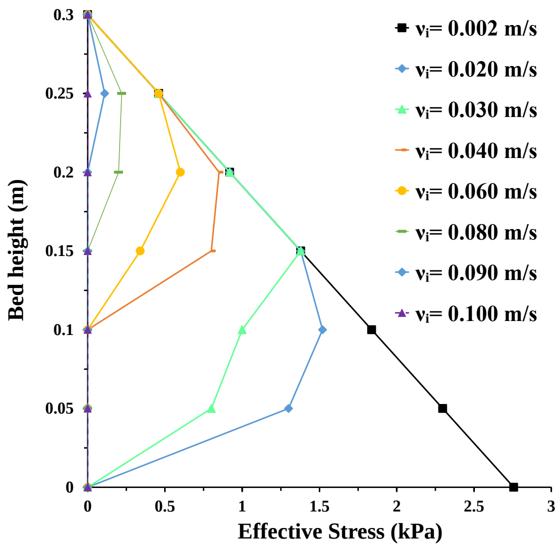

Bed height (m)
0.3
0.25
0.2
0.15
0.1
0.05
0
0
0.5
1
1.5
2
2.5
3
Effective Stress (kPa)
νi= 0.002 m/s
νi= 0.020 m/s
νi= 0.030 m/s
νi= 0.040 m/s
νi= 0.060 m/s
νi= 0.080 m/s
νi= 0.090 m/s
νi= 0.100 m/s

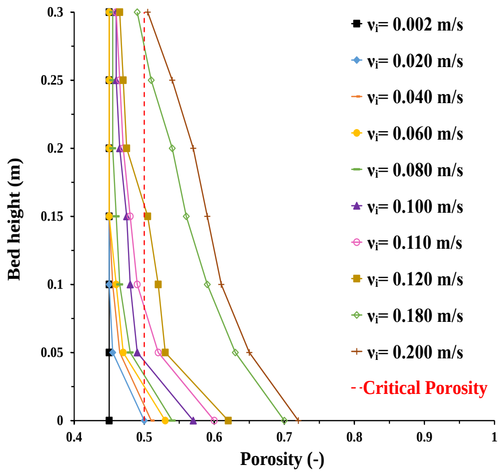

(a) ***o*= 2.5 mm**

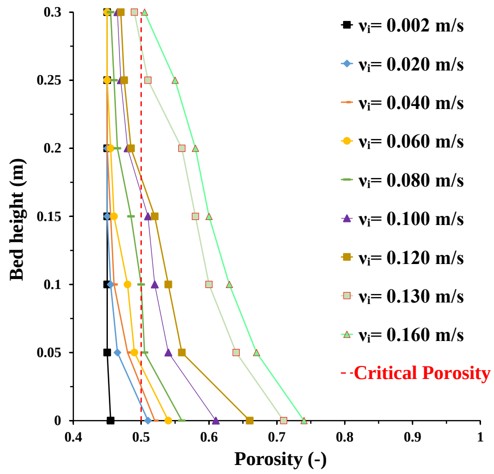

(b) ***o*= 5.0 mm**

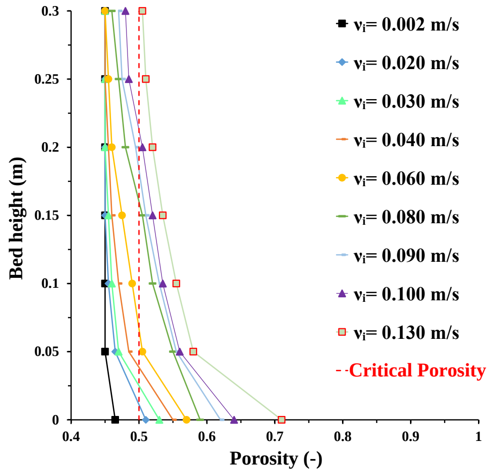

(c) ***o*= 7.5 mm**

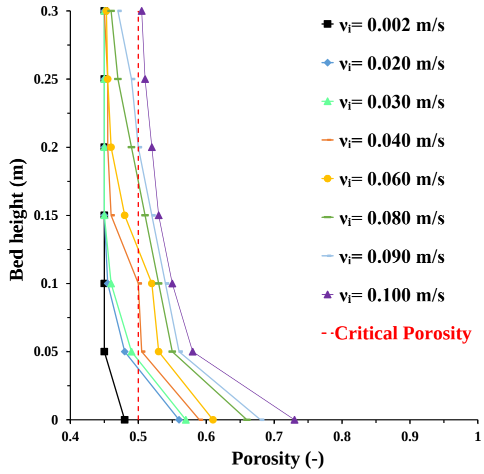

(d) ***o*= 10.0 mm**

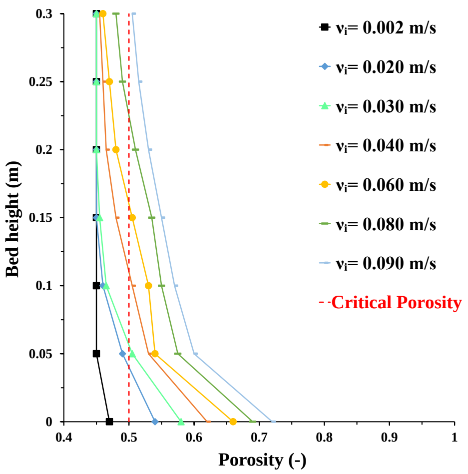

(e) ***o*= 12.5 mm**

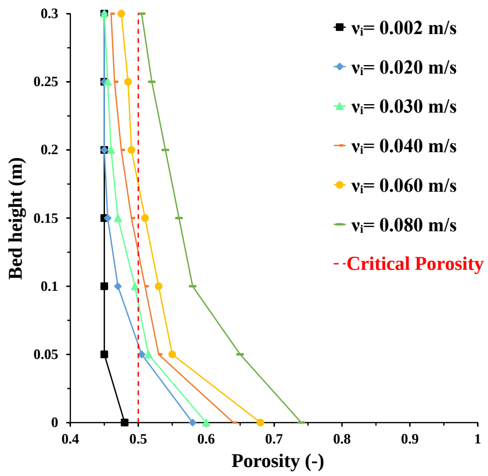

(f) ***o*= 15.0 mm**

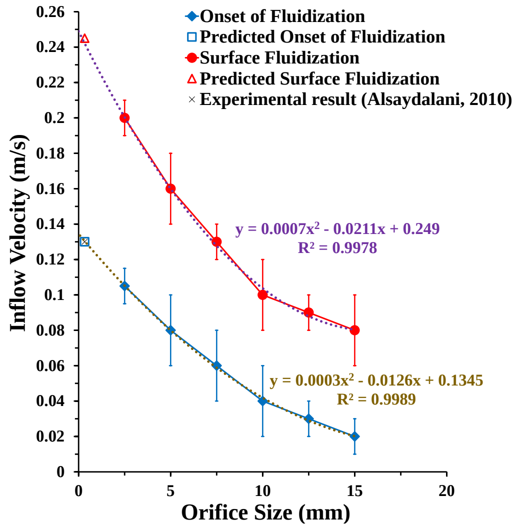
Onset of Fluidization
Predicted Onset of Fluidization
Surface Fluidization
Predicted Surface Fluidization
Experimental result (Alsaydalani, 2010)
y = 0.0007x² - 0.0211x + 0.249
R² = 0.9978
y = 0.0003x² - 0.0126x + 0.1345
R² = 0.9989
Inflow Velocity (m/s)
Orifice Size (mm)
0.26
0.24
0.22
0.2
0.18
0.16
0.14
0.12
0.1
0.08
0.06
0.04
0.02
0
0
5
10
15
20

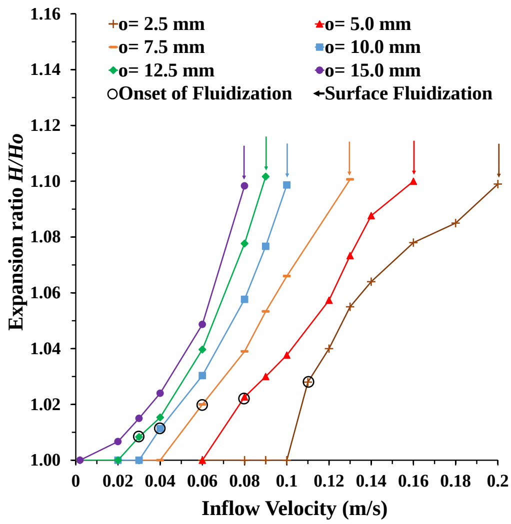

o= 2.5 mm
o= 5.0 mm
o= 7.5 mm
o= 10.0 mm
o= 12.5 mm
o= 15.0 mm
Onset of Fluidization
Surface Fluidization
Expansion ratio H/Ho
Inflow Velocity (m/s)
1.16
1.14
1.12
1.10
1.08
1.06
1.04
1.02
1.00
0
0.02
0.04
0.06
0.08
0.1
0.12
0.14
0.16
0.18
0.2

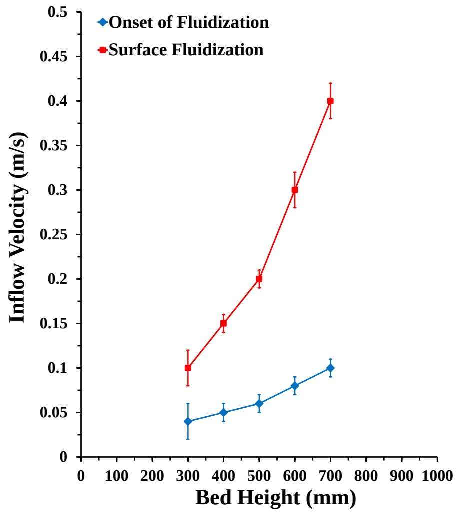

Onset of Fluidization
Surface Fluidization
Inflow Velocity (m/s)
0.5
0.45
0.4
0.35
0.3
0.25
0.2
0.15
0.1
0.05
0
0
100
200
300
400
500
600
700
800
900
1000
Bed Height (mm)

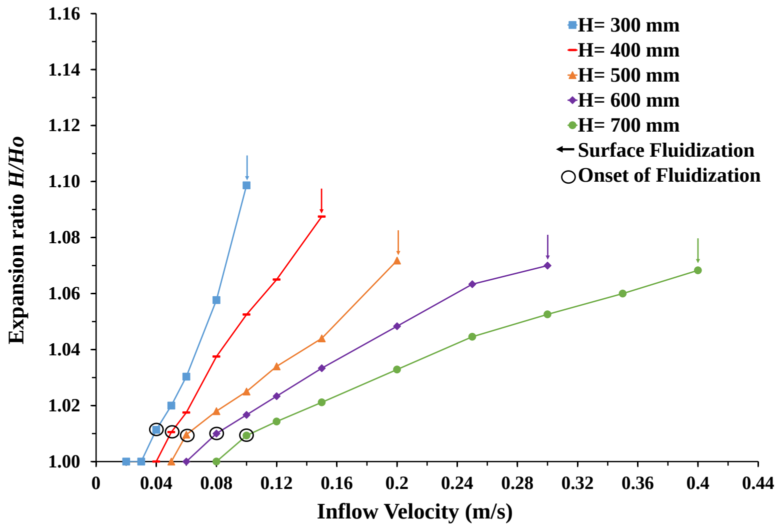
1.16
1.14
1.12
1.10
1.08
1.06
1.04
1.02
1.00
Expansion ratio H/Ho
0
0.04
0.08
0.12
0.16
0.2
0.24
0.28
0.32
0.36
0.4
0.44
Inflow Velocity (m/s)
H= 300 mm
H= 400 mm
H= 500 mm
H= 600 mm
H= 700 mm
Surface Fluidization
Onset of Fluidization

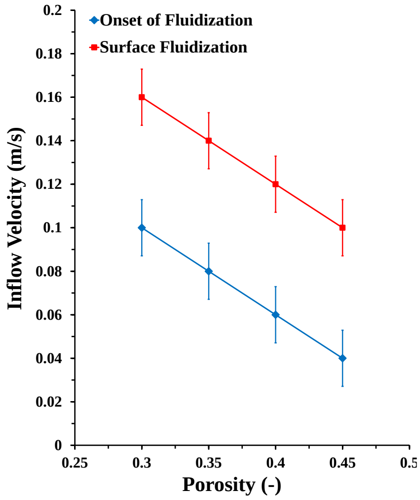

(a)

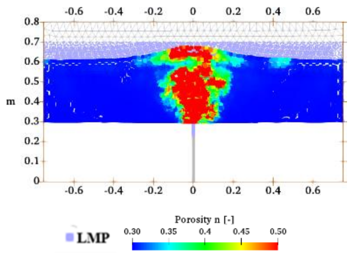

(b) n = 0.30; $v_{is} = 0.16\ m/s$

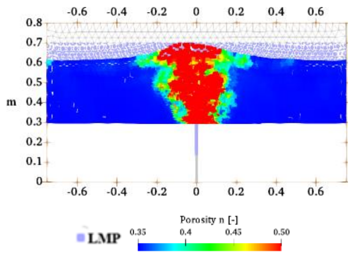

(c) n = 0.35; $v_{is} = 0.14\ m/s$

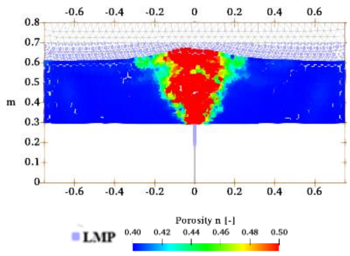

(d) n = 0.40; $v_{is} = 0.12\ m/s$

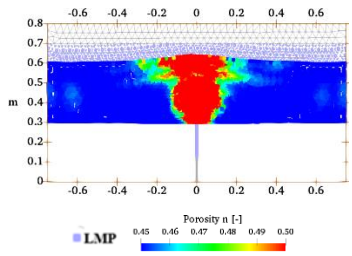

(e) n = 0.45; $v_{is} = 0.10\ m/s$

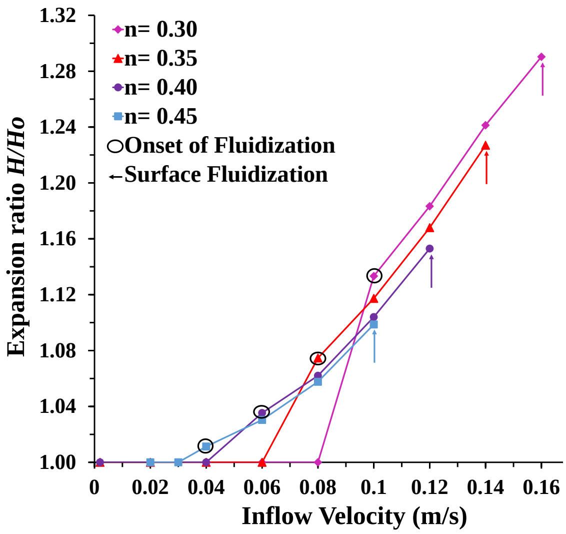

(a)

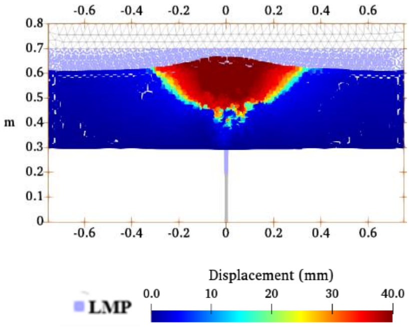

(b) n $= 0.30$; $v_{is} = 0.16\ m/s$

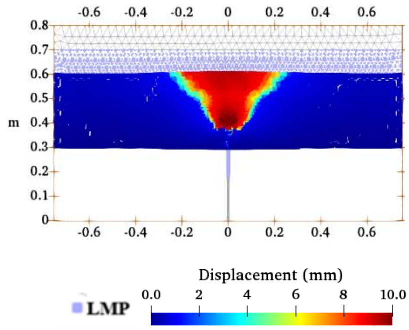

(c) n $= 0.45$; $v_{is} = 0.10\ m/s$